51st AIAA Aerospace Sciences Meeting including the New Horizons Forum and Aerospace Exposition
07 - 10 January 2013, Grapevine (Dallas/Ft. Worth Region), Texas

AIAA 2013-0007

Aeroacoustics of Three-Stream High-Speed Jets from Coaxial and Asymmetric Nozzles

Dimitri Papamoschou[1], Andrew D. Johnson[2], and Vincent Phong[3]
University of California, Irvine, Irvine, CA 92697

The development of three-stream variable cycle turbofan engines provides an opportunity for noise reduction by optimizing the exhaust conditions of the secondary and tertiary streams. This includes adjustment of the velocity ratios and, more importantly, reshaping of the nozzle. The paper reviews an experimental study of subscale three-stream nozzles, rapid-prototyped with high accuracy and operating at high specific thrust. Far-field noise surveys were collected using a 24-microphone array. For low-bypass configurations, applicable to supersonic aircraft, a coaxial configuration offers no significant noise benefit compared to the single-stream exhaust. Configurations with offset secondary or tertiary streams offer significant noise reduction in the direction of the thicker flow. For bypass ratio around 0.5, reductions of 5.1 dB in overall sound pressure level and 4.2 dB in effective perceived noise level were attained.

I. Introduction

The operational envelope of supersonic aircraft favors the use of low bypass ratio propulsion systems. The resulting community noise levels can be very high and exceed federal and local regulations, especially during takeoff. At high power settings the main source of noise is mixing noise from large-scale turbulent structures, which causes Mach wave emission. The problem of supersonic jet noise suppression has resulted in large-scale research efforts and vast contributions in the literature. Here we mention selected works in the area of multi-stream jets. The study of coaxial high-speed jets started in the 1970s[1] and has continued to be an area of active investigation[2-4]. Of particular interest in this study is the ability of a secondary flow to suppress Mach wave emission from a faster primary flow[5].

The presence of three exhaust streams in some of the more advanced engine cycles[6] opens up intriguing possibilities of noise reduction by tailoring the initial velocity profile of the jet. Initial experiments at NASA Glenn Research Center on three-stream nozzles noted a modest benefit of the tertiary stream under certain conditions[7]. Past experience with the “Mach wave elimination” method has shown that it is not particularly effective in a low-bypass coaxial exhaust[5], but can bring significant noise reduction in an offset-stream arrangement[8,9]. By extension, one may expect similar improvements if one or both outer streams in a three-stream nozzle are offset. This motivated a parametric study of coaxial and non-coaxial three-stream nozzles at conditions representative of low-bypass, high-performance jet engines. The results are primarily relevant to noise suppression for tactical military aircraft but may also relate to the development of supersonic business jets. The paper reviews the selection of engine cycles simulated experimentally, the three-stream nozzle designs, and the far-field acoustic results.

II. Conceptual Design of Nozzle

The objective of the nozzle design process was to generate models that would enable rapid and accurate testing of a variety of nozzles having characteristics compatible with the cycles of high-performance jet engines. The nozzles would need to fit the capacity and capability of the UCI Jet Aeroacoustics Facility depicted in Fig. 1. This is a dual-stream jet facility that delivers helium-air mixtures to the primary (core) and secondary (fan) flows of the nozzle. Helium-air mixtures simulate accurately the acoustics and fluid mechanics of hot jets[1,2]. To accommodate a third

[1] Professor, Department of Mechanical and Aerospace Engineering, dpapamos@uci.edu, Fellow AIAA.
[2] Postdoctoral Fellow, Department of Mechanical and Aerospace Engineering, adjohnso@uci.edu, Member AIAA.
[3] Graduate Student Researcher, Department of Mechanical and Aerospace Engineering, vphong@uci.edu, Student Member AIAA.

stream, the supply of the third stream is the same as that of the second stream with a pressure drop device to independently control the total pressure.

The resulting conceptual nozzle design is shown in Fig. 2. The pressure drop for the tertiary stream is enabled by a perforated plate mounted at the entrance of the tertiary nozzle. The nozzle incorporates a fixed base section and removable attachment parts that include the variable-geometry portions of the nozzle. This approach was inspired by the nozzle arrangement used in a recent parametric study of noise reduction in dual stream turbofan nozzles using fan flow deflectors[3].

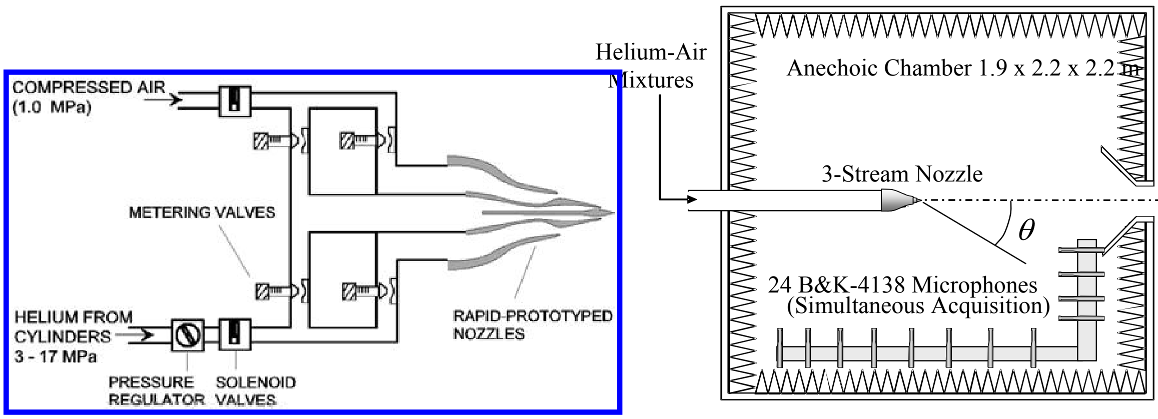

Fig. 1 Jet Aeroacoustics Facility at U.C. Irvine. Left: dual-stream apparatus using helium-air mixtures. Right: microphone array setup inside anechoic chamber.

The sub-millimeter tolerance requirements for the nozzle exit motivated a design where all the nozzle components are built in one piece, using the highest-resolution rapid prototyping available. The design comprises a fixed base on which a variety of nozzle attachments can be mounted, as illustrated in Fig. 2. When the attachment is secured to the base, the primary nozzle is supplied by an independently regulated helium-air mixture. An O-ring fitting prevents leakage to the outer two streams. The secondary and tertiary streams are fed by a second helium-air mixture. The supply is bisected in the attachment section with a perforated screen placed at the entrance of tertiary reservoir to control the tertiary total pressure, which is always lower than the secondary total pressure. The details of the nozzle design are reviewed in Section III.

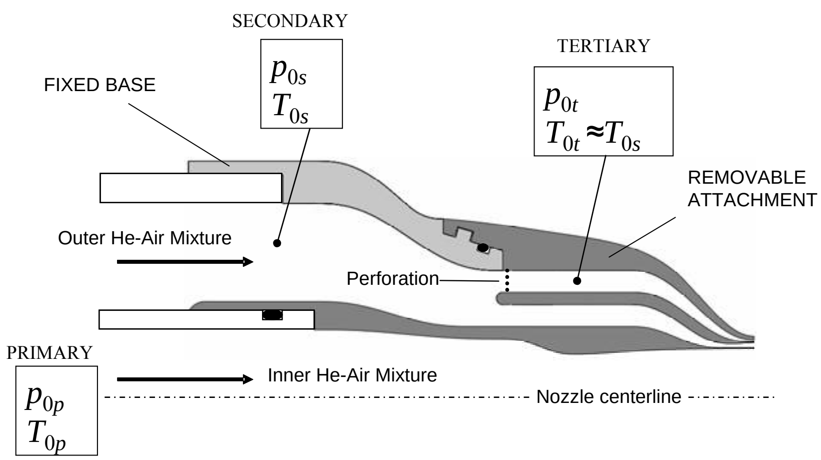

Fig. 2 Conceptual design of three-stream nozzle.

II. Engine Cycles Simulated

The cycle model is based on classic treatments in thermodynamic textbooks[10] combined with additional information published in recent literature[11-13], including the cooling of the high-pressure turbine with air bled by the compressor. Predictions of the model have agreed fairly well with published data on the performance of existing dual-stream engines. Figure 3 shows the principal elements of the three-stream gas turbine engine.

The engine parameters were calibrated to give exhaust conditions that reasonably represent a modern high-performance, low-bypass engine. This resulted in a turbine rotor inlet temperature RIT = 2100^o K, an overall pressure ratio OPR = 50, and turbine cooling using 22.5% of the core mass flow extracted at the exit of the compressor. Power extraction from the turbine to run auxiliary system was set at 2%. These parameters were fixed in the engine cycle analysis.

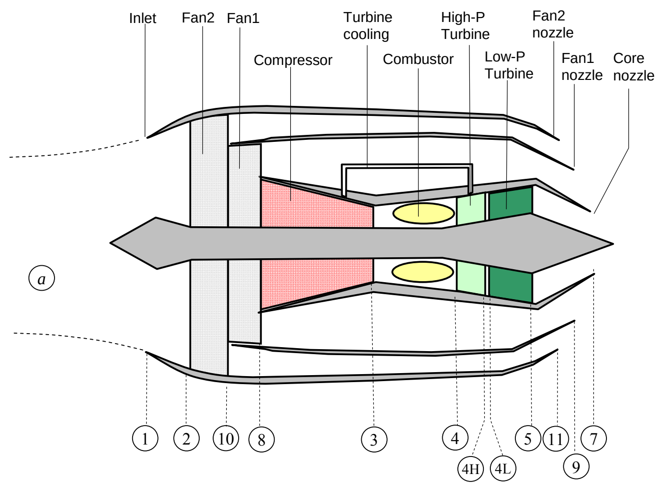

Fig. 3 Model for the engine cycle analysis.

Parametric studies of the engine cycle were done at fixed secondary bypass ratio (BPR$_s$=0.289) and fixed overall fan pressure ratio (FPR=4.78). The tertiary bypass ratio (BPR$_t$) and the tertiary fan pressure ratio (FPR$_t$, extracted from the overall fan pressure ratio) were variable. Table 1 summarizes the fixed and variable parameters of the engine cycle analysis.

Table 1: Engine cycle parameters

Parameter	Value
Overall pressure ratio (OPR)	50
Turbine inlet temperature (RIT)	2100^{o}K (3300^{o}F)
Core bleed air fraction for turbine cooling	0.225
Overall fan pressure ratio (FPR= FPR$_s$)	4.78
Secondary bypass ratio (BPR$_s$)	0.289
Tertiary fan pressure ratio (FPR$_t$)	Variable
Tertiary bypass ratio (BPR$_t$)	Variable

Increasing the tertiary fan pressure ratio FPR$_t$ or the tertiary bypass ratio BPR$_t$ results in a decline of the primary exhaust conditions (Mach number, velocity) because more power is extracted from the core flow. For fixed secondary fan pressure ratio and secondary bypass ratio, the secondary exhaust conditions experience very minor changes and remain virtually fixed at $A_s/A_p \approx 0.165$ and $U_s/U_p \approx 0.65$.

The variation of key engine parameters and exhaust conditions are examined in the form of contour plots versus the variables FPR$_t$ and BPR$_t$. Figure 4 plots the tertiary-to-primary exit area ratio (A_t/A_p), specific thrust, and thrust specific fuel consumption. The location of four cycle points of this report (**A**,**B**,**C**,**D**) are marked. Cycles **A**, **B**, and **C** are on a constant specific-thrust line and increasing FPR$_t$. Cycle **D** is a higher-BPR$_t$, lower-FPR$_t$ set point. In terms of noise reduction, particularly with offset-stream configurations, the area ratio A_t/A_p is perhaps the most crucial parameter. Cycle **D** has A_t/A_p=0.4, roughly double that of the other cycles.

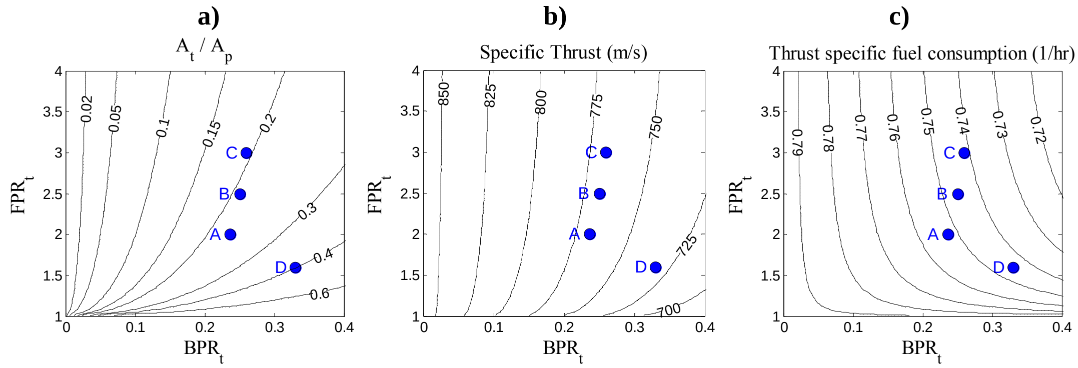

Fig. 4 Cycle analysis results versus tertiary bypass ratio and tertiary fan pressure ratio: a) tertiary-to-primary exit area ratio specific thrust; b) specific thrust; c) thrust specific fuel consumption.

The use of helium-air mixtures enables exact matching of the exit velocity and Mach number, with slight deviations in the density ratio[13]. The total temperatures (T_0) and nozzle temperature ratios (NTR= T_0/T_∞, where T_∞ is the ambient static temperature) used in this report refer to *equivalent* temperatures, simulated using the helium-air mixtures. Equivalent temperature is defined here the temperature of a hot jet that produces the same velocity as the helium-air mixture jet, at the Mach number of the helium-air mixture jet. Because the helium-air mixture has a higher specific heat ratio γ higher than air, the NPR for a particular Mach number is slightly different from that for air.

A constraint in the nozzle design of Fig.1 was the common supply for the secondary and tertiary streams. Adjustment (reduction) in the total pressure of the tertiary stream was enabled by a restriction in the form of a perforated plate at the entrance of the tertiary nozzle. Consequently the total temperature of the tertiary stream was controlled by that of the secondary stream. This relation is an exact equality for the actual total temperatures and an approximate equality ($T_{0t} \approx T_{0s}$) for equivalent total temperatures, using helium-air mixtures, because of effects of the variable γ. The ramification of this aspect of the design (the total temperature of the tertiary stream being set by that of the secondary stream) is that one cannot match both the velocity and the Mach number of the tertiary stream. The selection here was to match the velocity as it is more pertinent to acoustics. Because the tertiary stream was "warmer" than its nominal cycle condition, it was run at a lower NPR (lower Mach number) than the cycle point in order to match the velocity. In summary, the nozzle setup enabled the following simulation of the cycle conditions:

- The velocity and Mach number of the primary stream were both matched.
- The velocity and Mach number of the secondary stream were both matched.
- The velocity of the tertiary stream was matched. The tertiary Mach number was slightly lower than the cycle point. This resulted in a moderately lower tertiary bypass ratio and nozzle pressure ratio compared to the actual cycle point.

Table 2 shows the conditions simulated experimentally for the four cycle points of Fig. 4.

Table 2. Set points based on experimental simulation of engine cycle

	Primary			Secondary					Tertiary				
Case	NPR	NTR	U_p (m/s)	BPR$_s$	NPR$_s$	NTR$_s$	U_s/U_p	A_s/A_p	BPR$_t$	NPR$_t$	NTR$_t$	U_t/U_p	A_t/A_p
A	4.50	4.13	905	0.258	4.67	1.65	0.645	0.168	0.129	1.69	1.62	0.396	0.215
B	4.39	4.11	895	0.257	4.67	1.65	0.652	0.166	0.150	2.13	1.62	0.470	0.193
C	4.28	4.08	887	0.257	4.67	1.65	0.659	0.164	0.171	2.60	1.62	0.529	0.180
D	4.59	4.08	910	0.257	4.67	1.65	0.641	0.164	0.243	1.45	1.62	0.313	0.398

III. Detailed Nozzle Design and Fabrication

A. Scaling

The subscale nozzle was designed to be compatible with existing flow rate capabilities of the UC Irvine aeroacoustic facility. Since the majority of mass flow is needed to supply the primary flow, the primary exit diameter was the driving dimension for the scaling process. Based on past experiments with supersonic helium-air mixtures, an exit diameter of 18.28 mm (0.72 in) was deemed appropriate[3]. The lip thickness of the nozzle was limited by the manufacturing process and the resulting structural integrity of the nozzle walls. These constraints led to a thickness of 0.203 mm (0.008 in).

B. Nozzle Contours

The expansion part of the primary duct was designed using the method of characteristics (MOC) for uniform exit flow and included the effect of the displacement thickness of the boundary layer[15]. Upstream of the throat, the contour in the subsonic region was defined by a 5th-order polynomial that provided the desired fit between in inlet and throat sections. Given the very small dimensions of the secondary duct, an MOC method was deemed unnecessary and the entire contour was defined by 5th-order polynomials that provided the correct exit-to-throat area ratio. The tertiary nozzle, entirely subsonic, was also defined by 5th-order polynomials. All of the ducts terminated with zero slope. The secondary and tertiary nozzles had large contraction ratios. The inlet flow was thus very-low subsonic, allowing the placement of support struts without disturbing the exit flow.

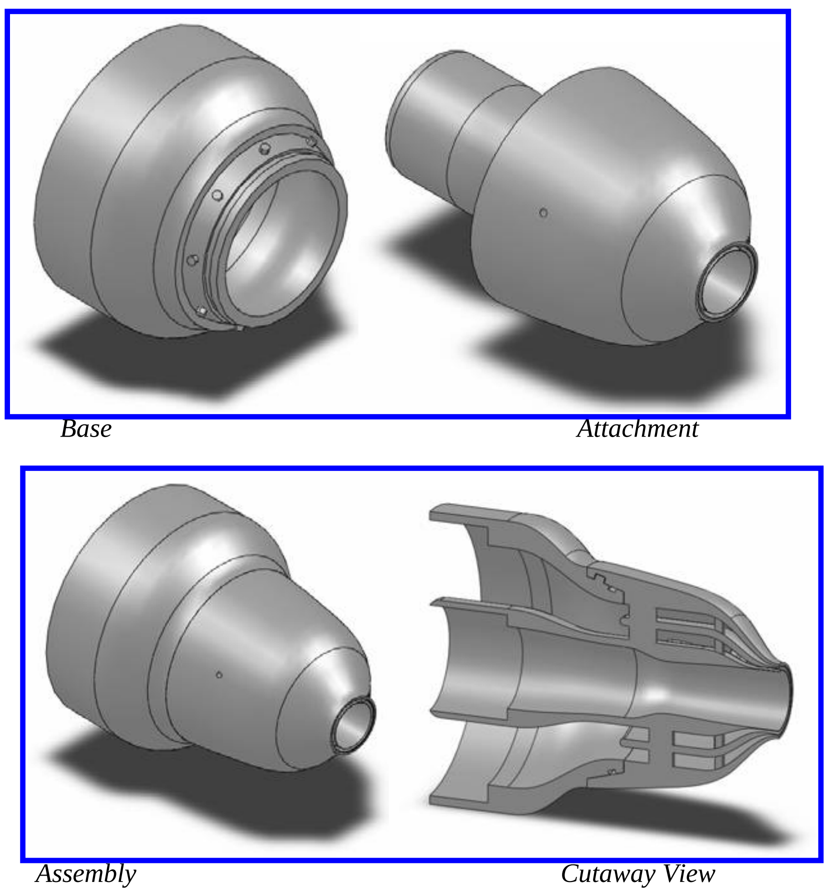

Fig. 5 CAD models of coaxial three-stream nozzle.

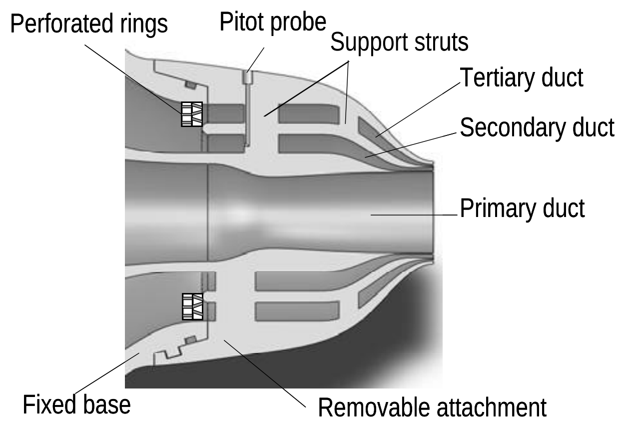

Fig. 6 Nozzle section showing internal structure and total-pressure measurement.

C. CAD Modeling
The coordinates of the nozzles were imported into Solidworks (Dassault Systemes) and integrated into a CAD model with fixed portions that comprise the interface with the base section and internal support struts. The CAD models of the base and attachment sections are shown in Fig. 5. Figure 6 shows a cross-sectional view.   The overall length of the assembly was 114.3 mm and the maximum diameter at the base is 95.0 mm. The interface between the base and the attachment utilized a notch and key style locking mechanism. The nozzle was secured in place by rotating the attachment piece with respect to the base. An O-ring situated in a groove on the base section ensured a leak-free internal flow path.

D. Control of Tertiary Stream
The pressure drop for the tertiary stream was controlled using two back-to-back perforated rings. The hole pattern on each ring allowed precise flow control by clocking the rings, as illustrated in Fig. 7. The rings were interlocking and the combination of the two rings sat firmly at the entrance of the tertiary nozzle.

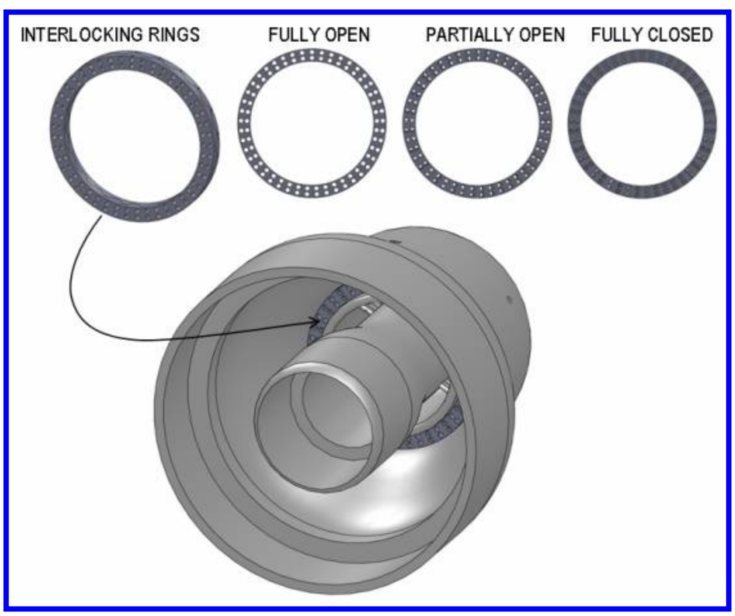

Fig. 7 Control of tertiary total pressure using clocking of two perforated rings.

E. Total Pressure Measurement

While measurement of the primary total pressure was straight-forward, measurement of the secondary and tertiary total pressures was non-trivial given the split described in Fig.2 and the overall complexity of the nozzle. Inserting Pitot tubes into the secondary and tertiary streams was deemed impractical. Instead, the total pressure measurement was integrated into the design of the nozzle. Just downstream of the base-attachment joint (Fig. 6) are six large support struts staggered in the axial direction. The perforated surface at the entrance of the tertiary nozzle is supported by three upstream struts. The three downstream struts are an ideal location for the Pitot pressure measurements since they provide a natural bridge to the internal ducting of the attachment piece. A 0.75-mm diameter channel was introduced in two of these struts; one to measure the secondary total pressure and the other to measure the tertiary total pressure. The channels begin at the outer surface of the attachment and follow an L-shaped path through the struts exiting facing upstream in their respective nozzle. The cross-sectional image of Fig. 6 illustrates the secondary Pitot port.

F. Nozzle Fabrication

The accuracy necessary in dealing with the small dimensions for this project required the state of the art in rapid prototyping technology. The base and attachment pieces were generated using an ultra fine resolution stereolithography method with build layers of 0.05 mm (FineLine Prototyping, Inc.) The material used was Accura 60 (3D Systems) with tensile and flexural strength in excess of 60 MPa. Figure 8 shows photographs of the completed parts. Figure 9 shows the exit detail of one of the nozzles; the intricacy and accuracy of the manufacturing is evident.

G. Nozzles of this Study

The specifications of the nozzles covered in this report are listed in Table 3. Figures 10 and 11 show the exit shapes for the coaxial and non-coaxial nozzles, respectively. Coaxial configurations were tested at all four cycle points. Nozzles with eccentric circular tertiary duct were tested for cycles **A**, **C**, and **D**. Two additional geometries were tested for cycle **D**. One had an ellipsoidal eccentric tertiary duct, designed to give uniform annulus thickness over azimuthal angles $-60^{o} \leq \phi \leq 60^{o}$; the annulus thickness distribution for this nozzle is compared to that of the round eccentric nozzle in Fig. 12. The other nozzle for cycle **D** had the eccentric ellipsoidal tertiary duct in combination with an eccentric round secondary duct.

Table 3 Nozzle specifications

Nozzle	Description	Exit dimensions in mm (Figs. 10,11)				
		A	B	C	D	E
A	Cycle A. All streams coaxial	18.29	0.72	0.84	-	-
B	Cycle B. All streams coaxial	18.29	0.72	0.76	-	-
C	Cycle C. All streams coaxial	18.29	0.72	0.72	-	-
D	Cycle D. All streams coaxial	18.29	0.72	1.51	-	-
AE	Cycle A. Eccentric tertiary duct	18.29	0.72	1.68	0.00	-
CE	Cycle C. Eccentric tertiary duct	18.29	0.72	1.40	0.00	-
DE	Cycle D. Eccentric tertiary duct	18.29	0.72	3.02	0.00	-
DEX	Cycle D. Eccentric ellipsoidal tertiary duct	18.29	0.72	2.76	0.00	-
DEX2	Cycle D. Eccentric ellipsoidal tertiary duct and eccentric secondary duct	18.28	1.44	2.76	0.00	0.00

A = Diameter of primary (inner) duct.
B = Thickness of secondary-duct annulus (maximum thickness for eccentric configuration).
C = Thickness of tertiary-duct-annulus (maximum thickness for eccentric configuration).
D = Minimum thickness of tertiary-duct annulus.
E = Minimum thickness of secondary-duct annulus.

a)

b)

Fig. 8 Pictures of a) base section and b) complete nozzle.

Fig. 9 Picture of exit of nozzle DEX2.

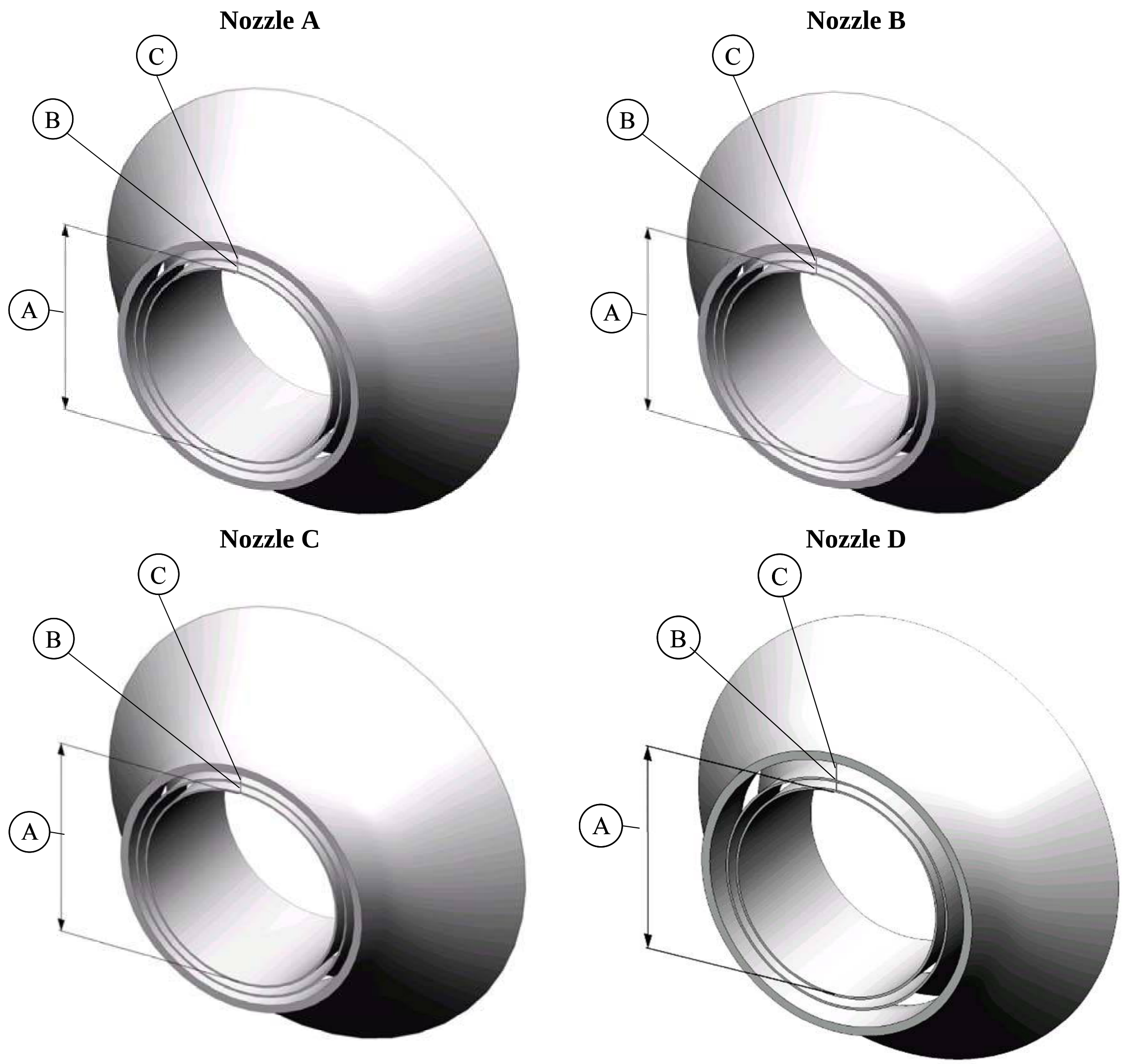

Fig. 10 Coaxial nozzles tested.

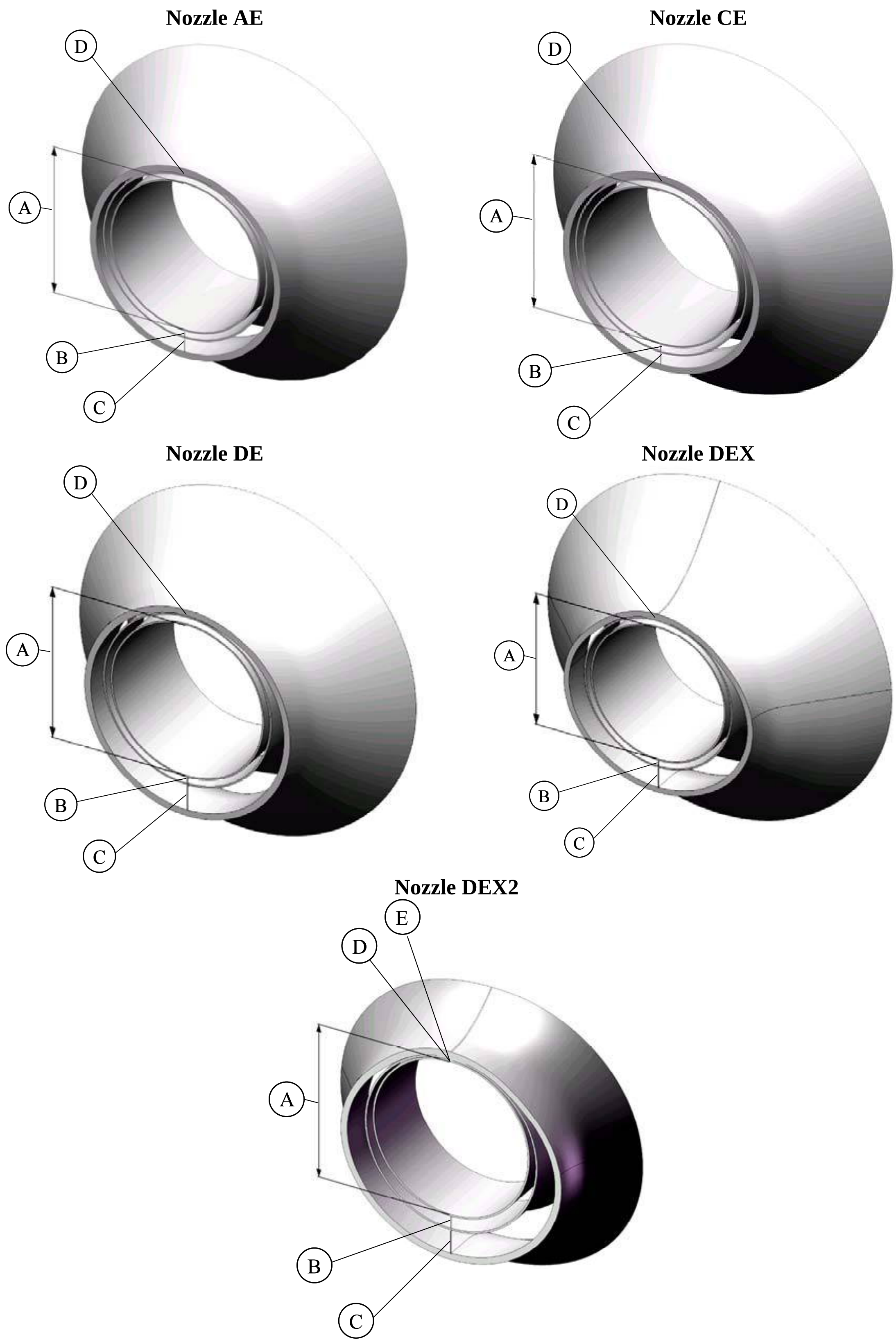

Fig. 11 Eccentric configurations tested.

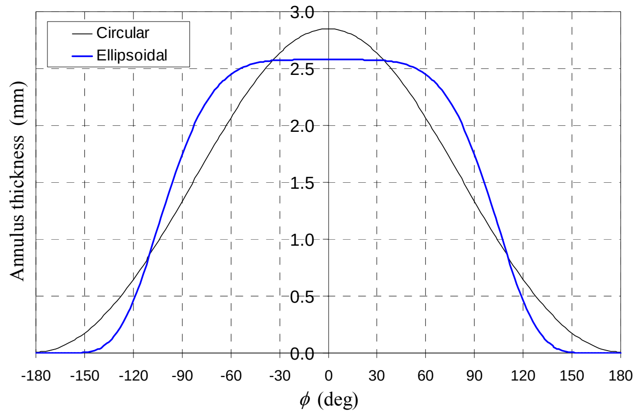

Fig. 12 Azimuthal distribution of annulus thickness for eccentric circular tertiary duct (nozzle DE) and eccentric ellipsoidal tertiary duct (nozzle DEX).

IV. Aeroacoustic Testing

Noise measurements were performed in the aeroacoustic facility shown in Fig. 1. The microphone array consists of twenty four 1/8-in condenser microphones (Bruel & Kjaer, Model 4138) with frequency response up to 120 kHz. For acoustic surveys, the microphones were arranged with twelve on a downward arm (azimuth angle $\phi = 0^o$) and twelve on a sideline arm (azimuth angle $\phi = 60^o$). Figure 1 depicts the configuration of the downward arm; the sideline arm is practically identical. On each arm, the polar angle θ ranged approximately from 20 to 120 deg relative to the jet axis. This arrangement enabled simultaneous measurement of the downward and sideline noise at all the polar angles of interest. The microphones were connected, in groups of four, to six conditioning amplifiers (Bruel & Kjaer, Model 2690-A-0S4). The 24 outputs of the amplifiers were sampled simultaneously, at 250 kHz per channel, by three 8-channel multi-function data acquisition boards (National Instruments PCI-6143) installed in a Dell Precision T7400 computer with a Xeon quad-core processor. National Instruments LabView software was used to acquire the signals. The temperature and humidity inside the anechoic chamber were recorded to enable computation of the atmospheric absorption. The microphone signals were conditioned with a high-pass filter set at 300 Hz. Narrowband spectra were computed using a 4096-point Fast Fourier Transform yielding a frequency resolution (Δf = 61 Hz). The spectra were corrected for microphone actuator response, microphone free field response and atmospheric absorption. Integration of the corrected spectra gives the overall sound pressure level (OASPL).

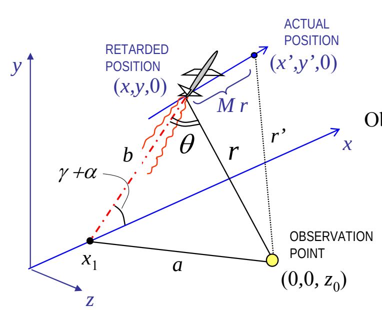

Aircraft flying with Mach number M, angle of attack α, and climb angle γ

Observation distance and polar emission angle

$$r' = \sqrt{x'^2 + y'^2 + z_0^2}$$

$$r = \sqrt{x^2 + y^2 + z_0^2}$$

$$\tan(\theta/2) = \sqrt{\frac{(p-b)(p-r)}{p(p-a)}}$$

where

$$x_1 = x - y/\tan(\gamma+\alpha)$$

$$a = \sqrt{x_1^2 + z_0^2}$$

$$b = y/\sin(\gamma+\alpha)$$

$$p = \frac{1}{2}(a+b+r)$$

CONDITIONS FOR EVALUATON OF PNL		
	SIDELINE	DOWNWARD
Lateral distance, z_o=	1476 ft	0 ft
Altitude at x=0	1500 ft	2000 ft
Angle of attack, α=	10 deg	10 deg
Climb angle, γ=	20 deg	20 deg
Flight Mach, M=	0.300	0.300

Fig. 13 Geometric relations and conditions for assessment of perceived noise level.

The perceived noise level (PNL) and effective perceived noise level (EPNL) are used as the primary metrics for evaluating noise reduction. They are calculated based on a full-scale primary diameter of 24 in (0.610 m), flight Mach number of 0.30, engine angle of attack of 10^{o}, and climb angle of 20^{o}. Figure 13 summarizes the conditions and variables used in the evaluation of PNL. Details of the PNL calculation procedure are available in Ref. 2.

V. Results

The acoustic results are divided in two parts. The first part compares the jet with primary flow alone to the three-stream coaxial jet. The purpose of this comparison is to examine the effects of the secondary and tertiary flows, arranged symmetrically, on the acoustic emission. The second part compares the acoustic emission of coaxial and non-coaxial three-stream jets. The comparisons will be provided in terms of an "acoustic summary" comprising the following metrics (see Fig. 14, for example): narrowband SPL spectra in the direction of peak emission and at large polar angle; OASPL versus polar angle; and PNL versus flyover time. For asymmetric nozzles, these quantities will be provided in the downward ($\phi=0^{o}$) and sideline ($\phi=60^{o}$) azimuthal directions.

A. Three-Stream Coaxial Jet versus Primary Jet Alone

To assess the potential of Mach wave suppression due to the operating conditions alone, we compare the coaxial three-stream jet with the jet comprising the primary flow alone. Figures 14-17 display the relevant acoustic summaries for cycles **A** through **D**. For cycles **A**, **B**, and **C** there are small increases in spectral levels and OASPL at angles lower than the angle of peak emission, followed by no change or a very slight decrease for the larger angles. The overall levels (OASPL, EPNL) increase by about 1 dB. This is on the same order as the noise increase due to the thrust increase associated with the introduction of the secondary and tertiary streams. We conclude that, for cycles **A**-**C**, there is no evidence of noise attenuation by the secondary and tertiary flows. This is due to the very small thicknesses of the secondary and tertiary flows. For cycle **D**, which has a thicker tertiary flow, we note very slight increases at the small angles followed by moderate reductions at the large angles. The OASPL and EPNL do not change significantly. On a constant-thrust basis, this flow is ~ 1 dB quieter. So there is some evidence here of noise suppression due to the reduced shear by the secondary and, particularly, the tertiary streams.

B. Three-Stream Non-Coaxial versus Coaxial Jet.

Figures 18-23 compare three-stream coaxial jets with three-stream jets having eccentric tertiary duct for cycles **A**, **C**, and **D**. The comparisons now include the downward and sideline azimuthal directions. For cycles **A** and **C**, offsetting the tertiary duct causes appreciable reductions in the peak spectral levels in the downward direction, with associated decreases in peak OASPL and EPNL of around 1.5 dB. The sideline direction experience a modest increase (cycle **A**) or no change (cycle **C**). Doubling the tertiary area, cycle **D**, leads to significant improvements in the downward noise reduction (Fig.22). The EPNL and peak OASPL both decline by ~3 dB. Noise in the sideline direction is practically unchanged.

The special nozzles DEX and DEX2 are now reviewed (Figs. 24-27). Figure 24 shows that nozzle DEX, with ellipsoidal-eccentric tertiary duct, achieves roughly the same downward reduction as its circular-eccentric counterpart (nozzle DE). The sideline noise shows a modest improvement over nozzle DE (compare Figs. 23 and 25). This indicates that the approach of increasing the sideline thickness of the tertiary annulus has a benefit on sideline noise, albeit small in this design. In nozzle DEX2 the ellipsoidal-eccentric tertiary duct is combined with an eccentric secondary duct, both eccentricities being directed downward. The combination of the two eccentric ducts offers significant improvements in noise reduction, the EPNL and peak OASPL reducing by 4.2 dB and 5.1 dB, respectively, in the downward reduction. This combination also has a distinct benefit in the sideline reduction of 0.9 dB in EPNL and 1.0 dB in peak OASPL.

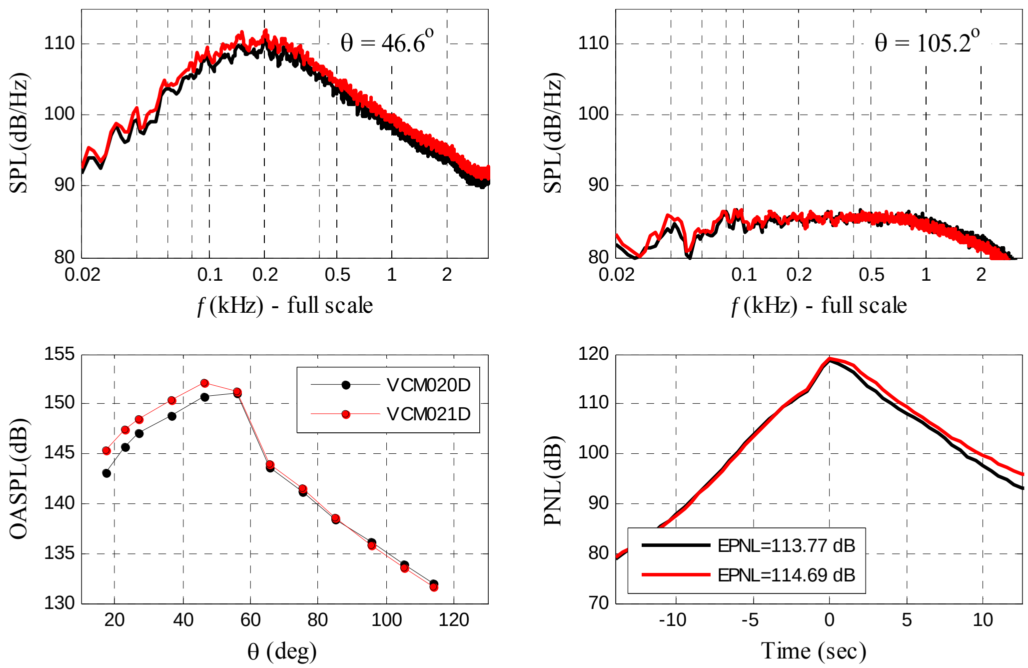

Fig. 14 Acoustic summary for coaxial Nozzle A (Cycle A). Primary stream alone (black) compared to coaxial three-stream jet (red). $\Delta OASPL_{max}$=1.0 dB; ΔEPNL=0.9 dB.

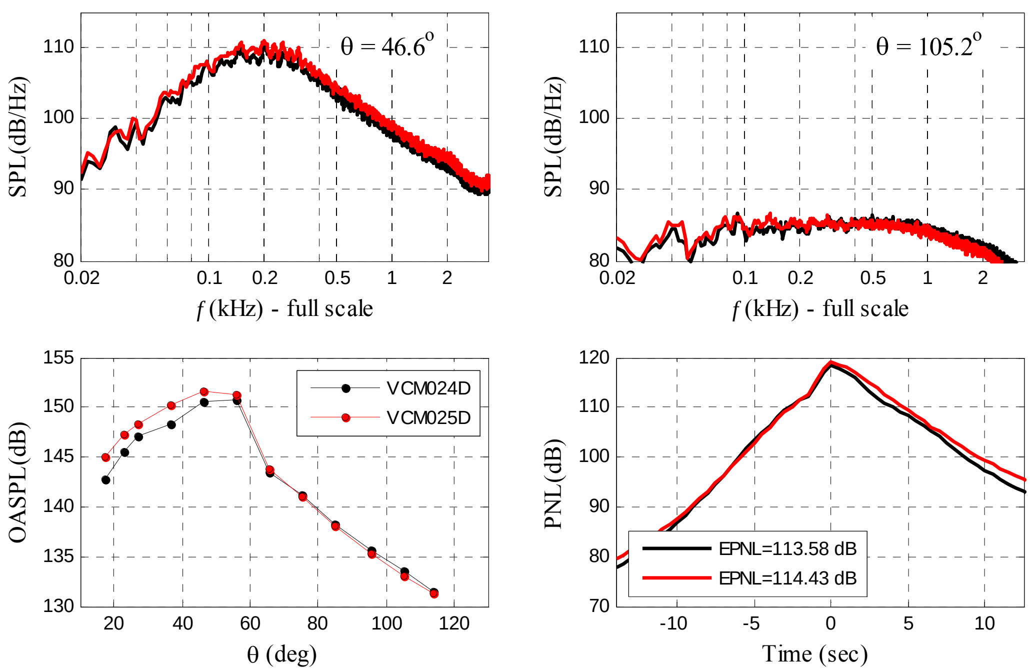

Fig. 15 Acoustic summary for coaxial Nozzle B (Cycle B). Primary stream alone (black) compared to coaxial three-stream jet (red). $\Delta OASPL_{max}$=0.8 dB; ΔEPNL=0.8 dB.

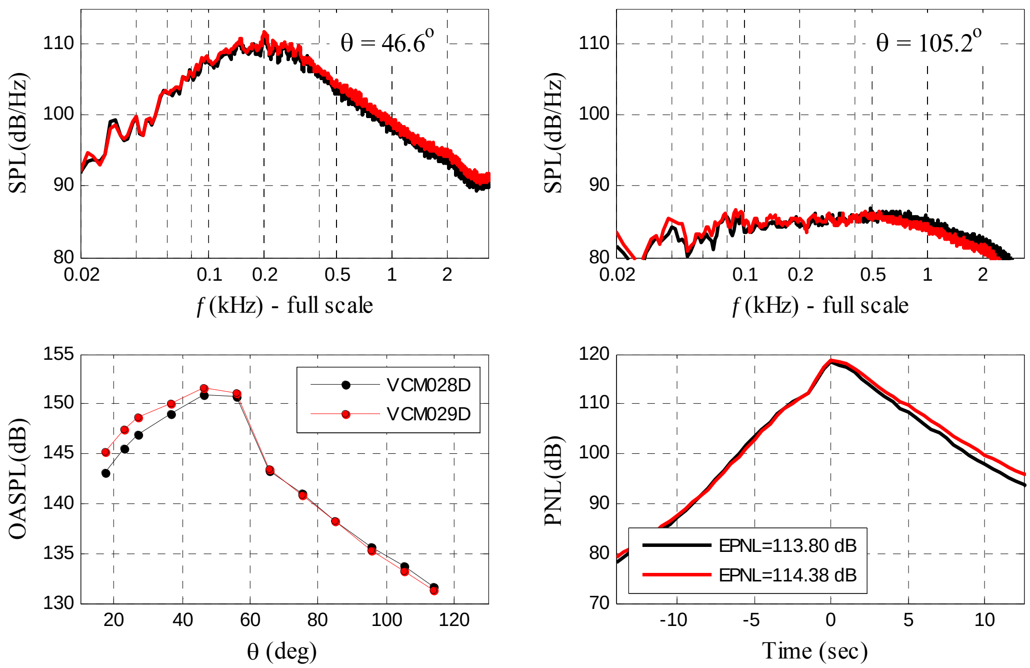

Fig. 16 Acoustic summary for coaxial Nozzle C (Cycle C). Primary stream alone (black) compared to coaxial three-stream jet (red). $\Delta OASPL_{max}$=0.6 dB; ΔEPNL=0.7 dB.

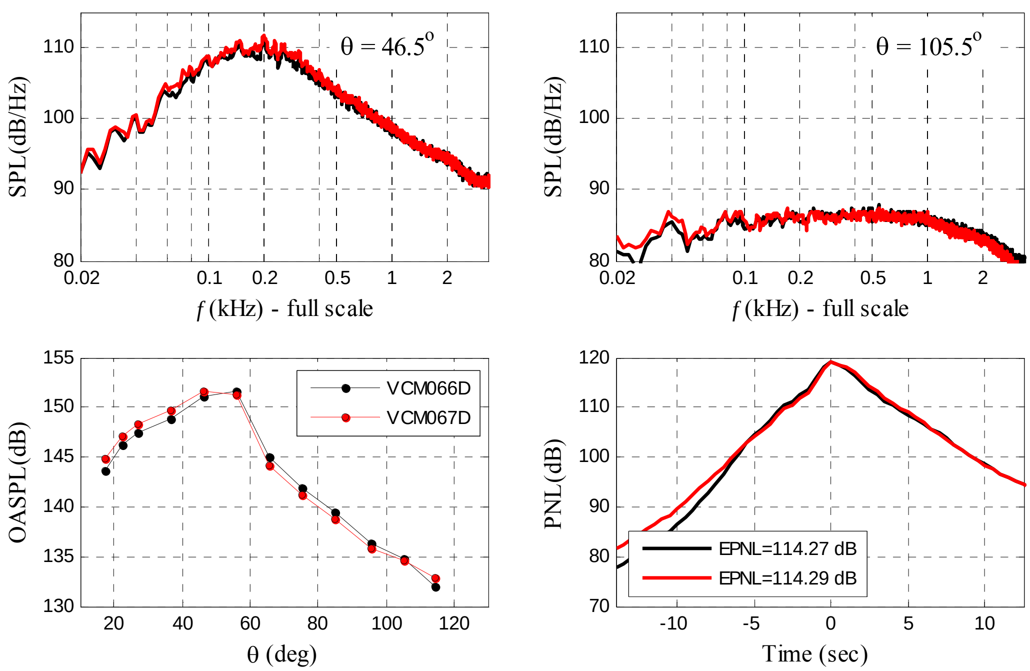

Fig. 17 Acoustic summary for coaxial Nozzle D (Cycle D). Primary stream alone (black) compared to coaxial three-stream jet (red). $\Delta OASPL_{max}$= -0.1 dB; ΔEPNL= 0.0 dB.

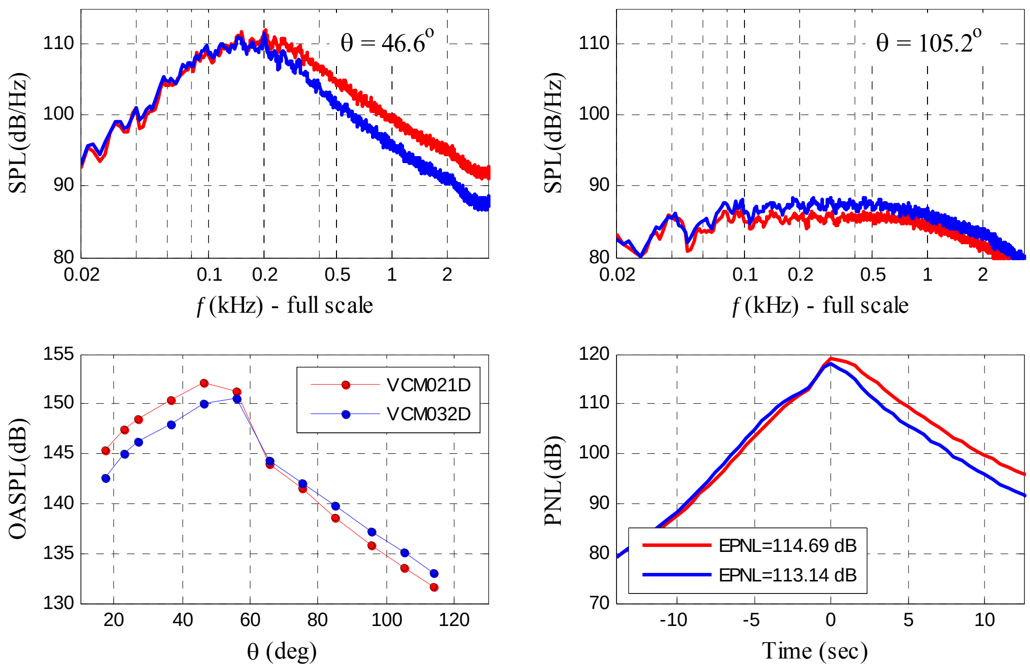

Fig. 18 Acoustic summary for nozzles A and AE (Cycle A) in the downward direction. Coaxial jet (red) compared to jet with eccentric tertiary flow (blue). $\Delta OASPL_{max}$= -1.5 dB; ΔEPNL= -1.5 dB.

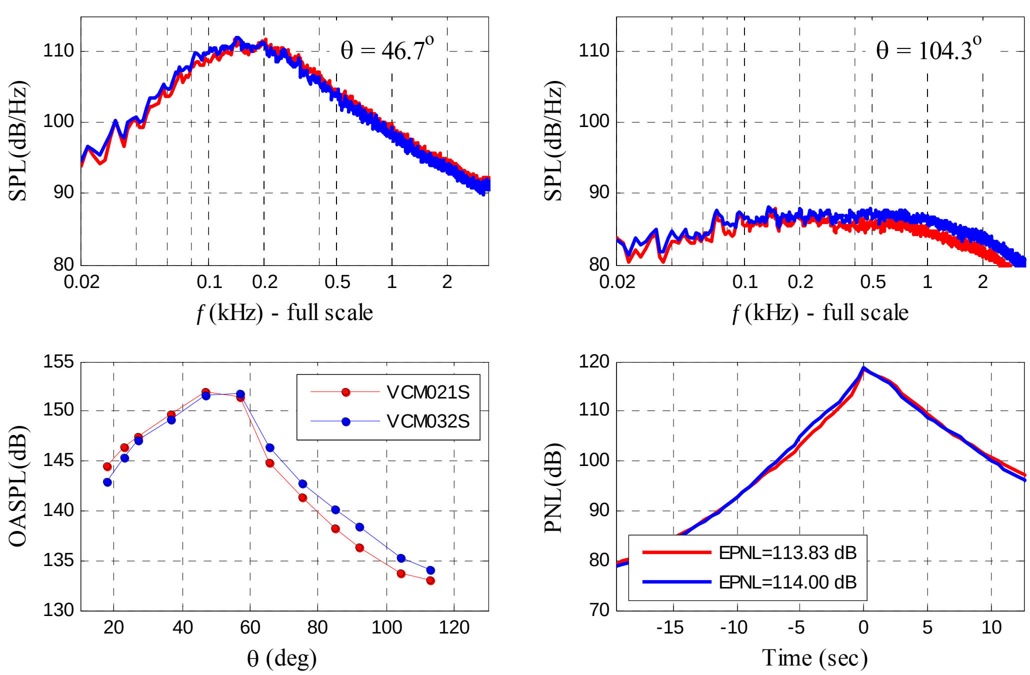

Fig. 19 Acoustic summary for nozzles A and AE (Cycle A) in the sideline direction. Coaxial jet (red) compared to jet with eccentric tertiary flow (blue). $\Delta OASPL_{max}$= -0.1 dB; ΔEPNL= -0.2 dB.

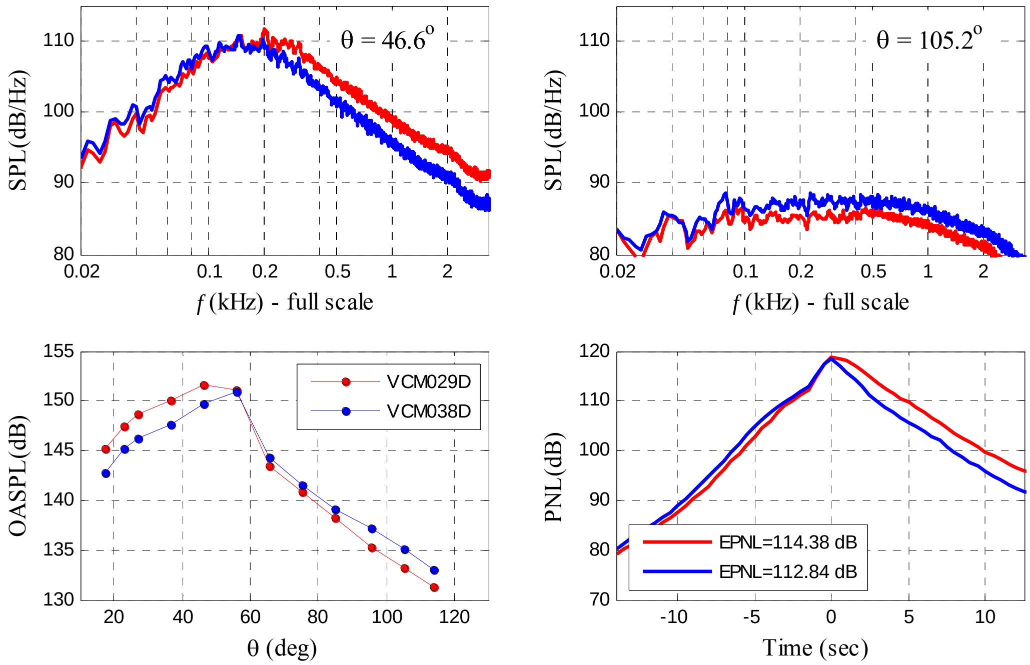

Fig. 20 Acoustic summary for nozzles C and CE (Cycle C) in the downward direction. Coaxial jet (red) compared to jet with eccentric tertiary flow (blue). $\Delta OASPL_{max}$= -0.8 dB; ΔEPNL= -1.5 dB.

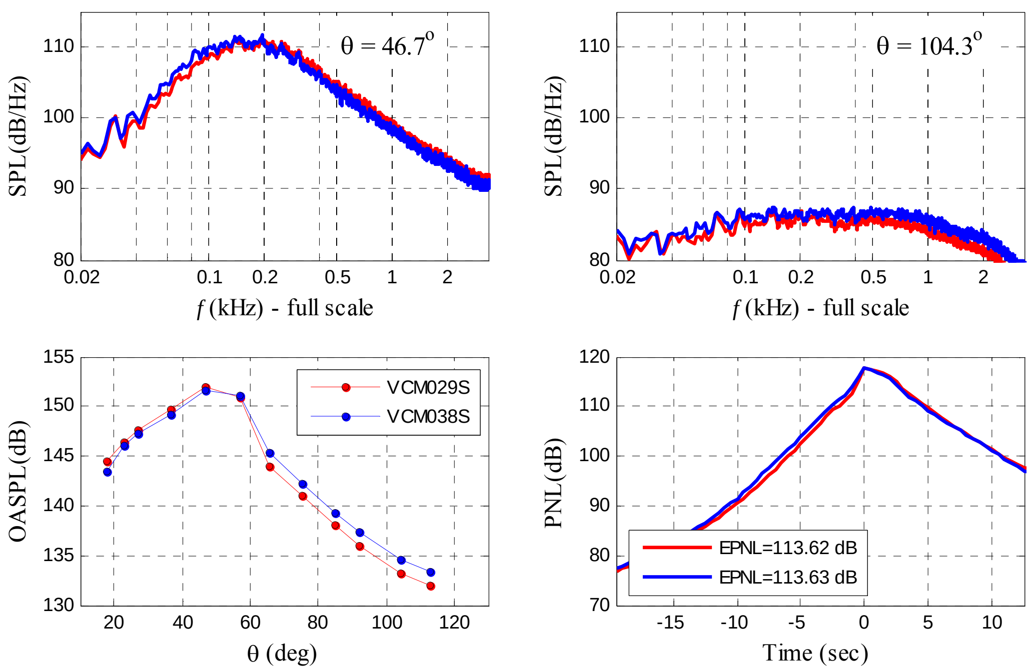

Fig. 21 Acoustic summary for nozzles C and CE (Cycle C) in the sideline direction. Coaxial jet (red) compared to jet with eccentric tertiary flow (blue). $\Delta OASPL_{max}$= -0.3 dB; ΔEPNL= 0.0 dB.

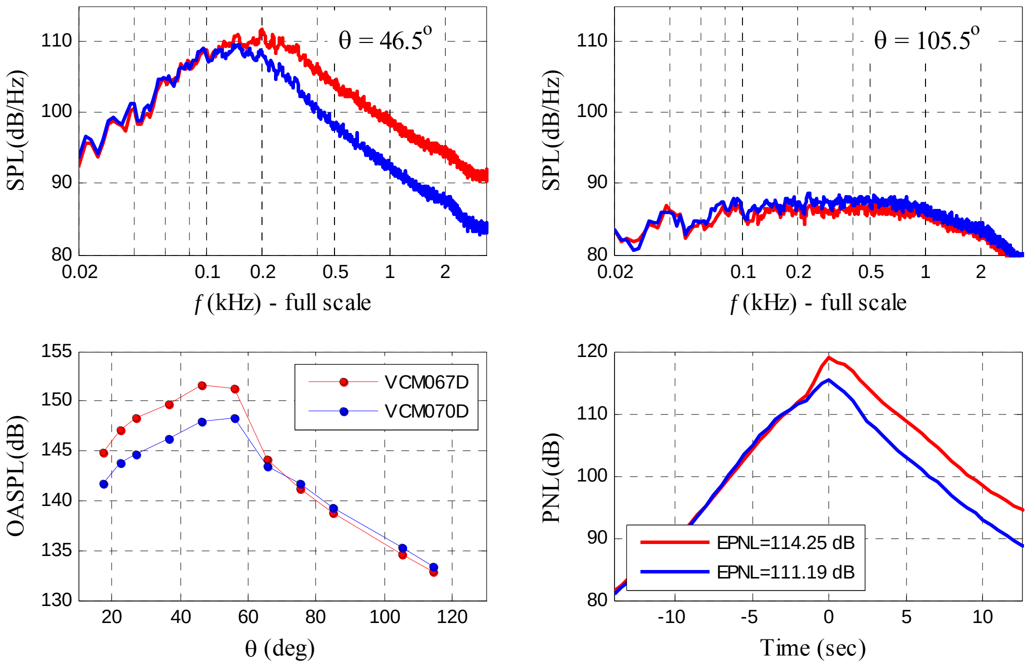

Fig. 22 Acoustic summary for nozzles D and DE (Cycle D) in the downward direction. Coaxial jet (red) compared to jet with eccentric tertiary flow (blue). $\Delta OASPL_{max}$= -3.3 dB; ΔEPNL= -3.1 dB.

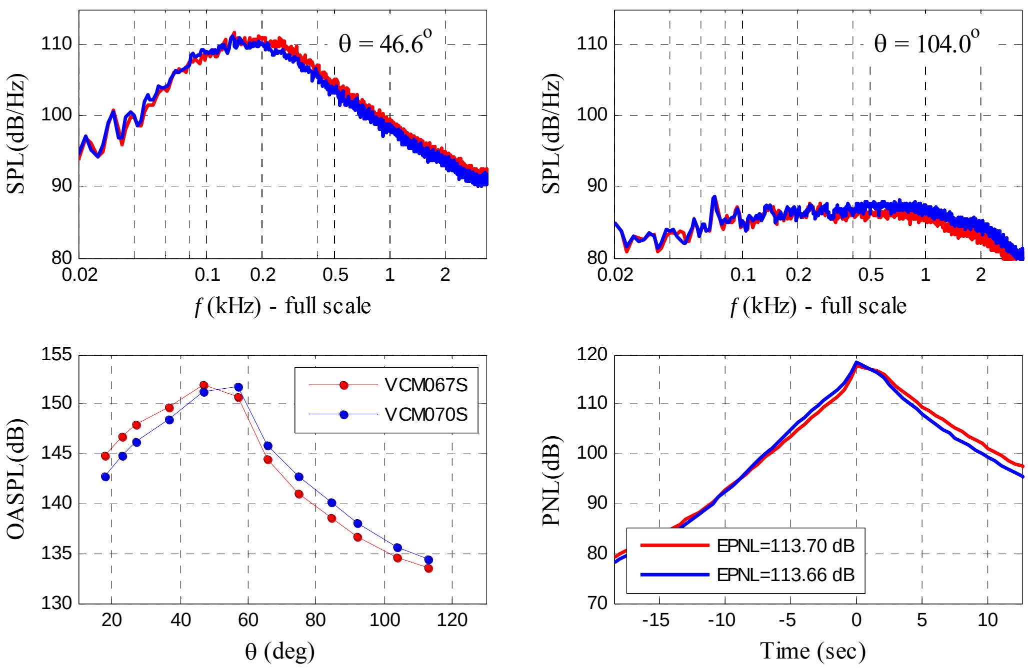

Fig. 23 Acoustic summary for nozzles D and DE (Cycle D) in the sideline direction. Coaxial jet (red) compared to jet with eccentric tertiary flow (blue). $\Delta OASPL_{max}$= -0.2 dB; ΔEPNL= 0.0 dB.

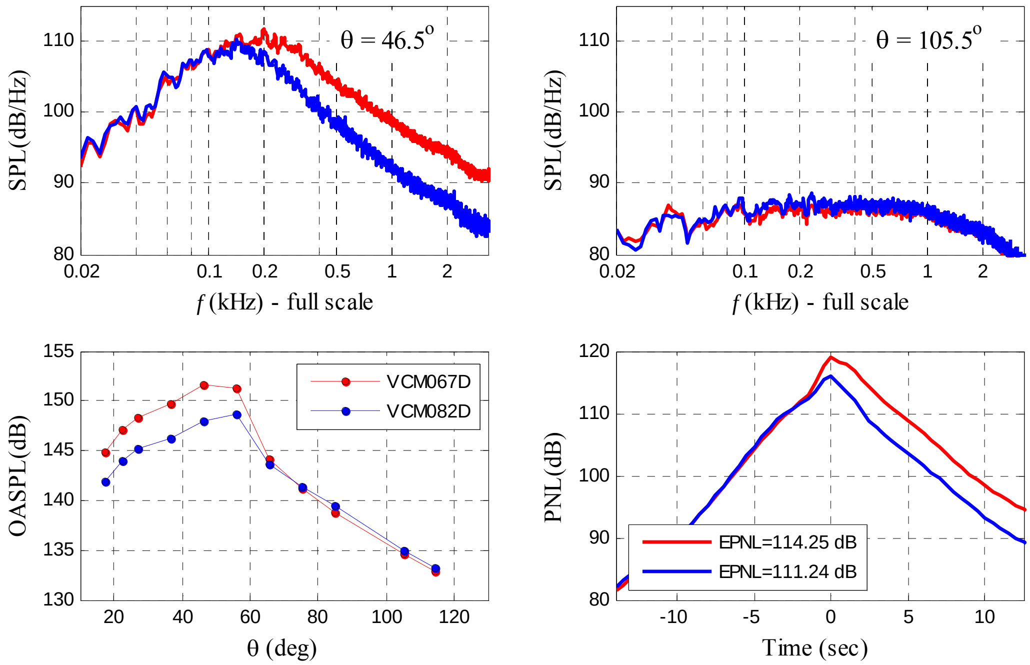

Fig. 24 Acoustic summary for nozzles D and DEX (Cycle D) in the downward direction. Coaxial jet (red) compared to jet with eccentric/ellipsoidal tertiary flow (blue). $\Delta OASPL_{max}$= -2.9 dB; $\Delta EPNL$= -3.1 dB.

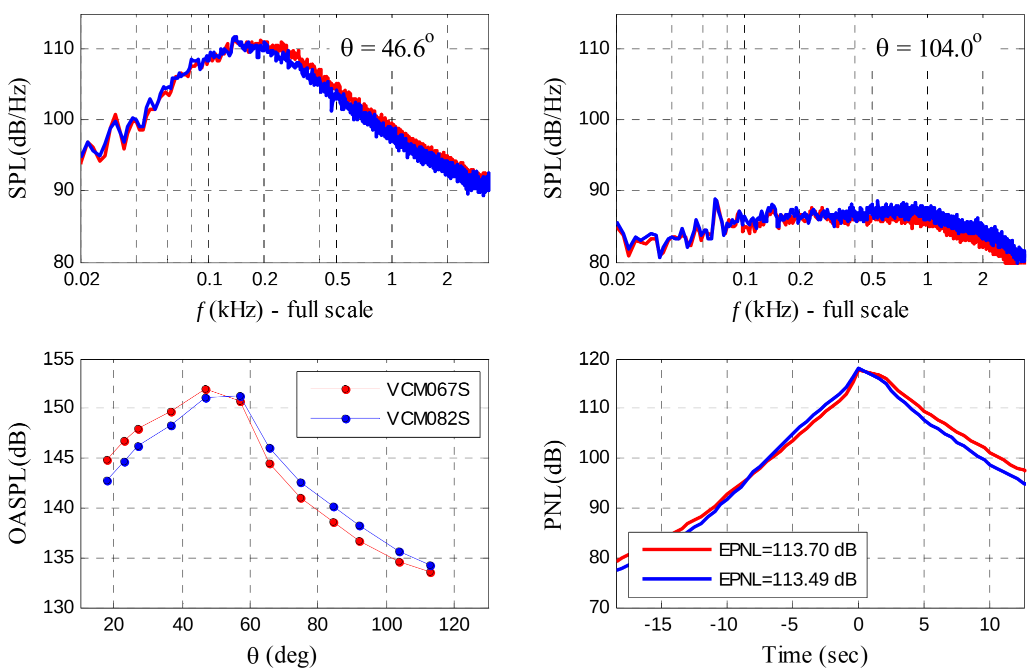

Fig. 25 Acoustic summary for nozzles D and DEX (Cycle D) in the sideline direction. Coaxial jet (red) compared to jet with eccentric/ellipsoidal tertiary flow (blue). $\Delta OASPL_{max}$= -0.8 dB; $\Delta EPNL$= -0.2 dB.

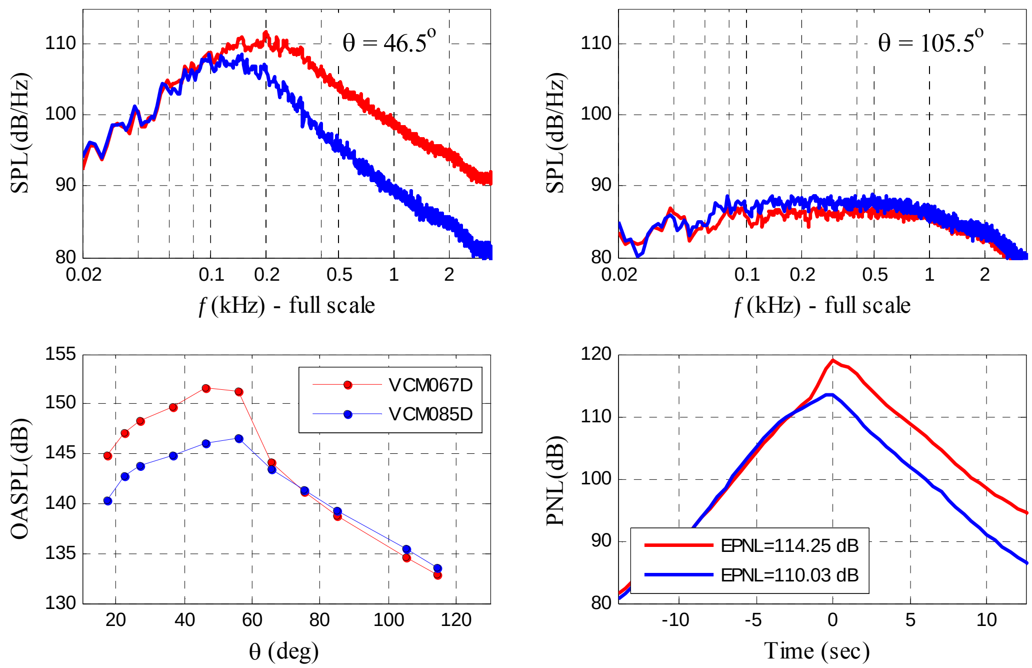

Fig. 26 Acoustic summary for nozzles D and DE X2 (Cycle D) in the downward direction. Coaxial jet (red) compared to jet with eccentric/ellipsoidal tertiary flow and eccentric secondary flow (blue). ΔOASPL$_{max}$= -5.1 dB; ΔEPNL= -4.2 dB.

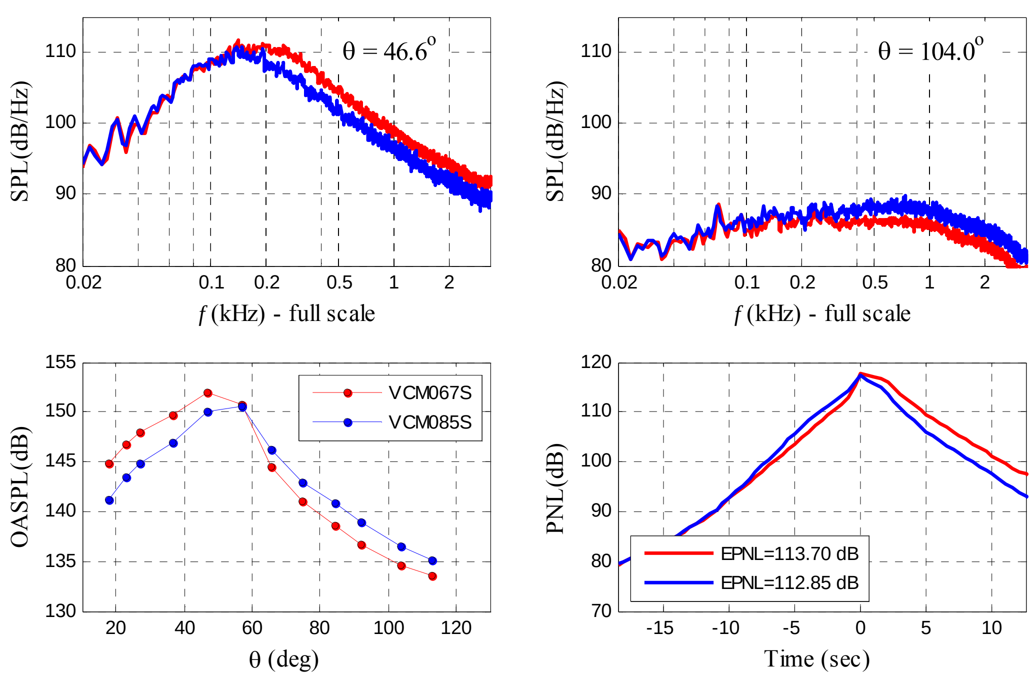

Fig. 27 Acoustic summary for nozzles D and DEX2 (Cycle D) in the sideline direction. Coaxial jet (red) compared to jet with eccentric/ellipsoidal tertiary flow and eccentric secondary flow (blue). ΔOASPL$_{max}$= -1.3 dB; ΔEPNL= -0.9 dB.

V. Conclusions

The experiments of this study provided an assessment of noise reduction from three-stream, high-speed jets by conducting a parametric investigation of round-coaxial and asymmetric nozzles. Intricate subscale nozzles were designed and manufactured using advanced stereolithographic methods. Following are the principal findings.

- For low-bypass-ratio coaxial jets with normal velocity profile, the conditions of the secondary and tertiary streams do not result in significant noise suppression. The annuli of the secondary and tertiary streams are too thin for these flows to penetrate far downstream in order to reduce the Mach wave source.
- Offset nozzle arrangements offer a significant noise benefit in the direction of the thickened flow, even at moderately low bypass ratios. In jets with combined bypass ratio around 0.4, an eccentric tertiary stream resulted in noise suppression (over the coaxial configuration) of 1.5 dB in EPNL in the direction of the thickened flow. Increasing the combined bypass ratio to ~0.5 improved this figure to ~3 dB. It is likely that further increases in the bypass ratio (more specifically, increases in the areas of the tertiary and secondary streams) will result in even larger reductions.
- The best configuration of this report comprised an eccentric ellipsoidal tertiary duct combined with an eccentric secondary duct (nozzle DEX2). It provided EPNL reductions of up to 4.3 dB in the downward direction (direction of thickened flows) and 0.9 dB in the sideline direction.

The success of the combined eccentricities in the tertiary and secondary ducts suggests that there is room for further noise reduction, at fixed bypass ratio, by optimal reshaping of these ducts. This concept may even extend to the primary duct. Optimization would be most effective using a combined experimental and computational effort.

Acknowledgment

We gratefully acknowledge the support by Rolls-Royce contract RR51848, monitored by Dr. William Dalton.

References

1. Dosanjh, D., Ahuja, J., Bassiouni, M., Bhutiani, P., "Supersonic Jet Noise Suppression by Coaxial Cold/Heated Jet Flows," AIAA Paper 76-507, July 1976.
2. Tanna, H. K., "Coannular Jets–Are They Really Quiet and Why?" *Journal of Sound and Vibration*, Vol. 72, No. 1, 1980, pp. 97–118.
3. Dahl, M.D. and Papamoschou, D., "Supersonic Coaxial Jets: Noise Predictions and Measurements," *AIAA Journal*, Vol. 38, No.4, 2000, pp. 584-591.
4. Tinney, C. and Jordan, P., "Coupling Mechanisms in a Co-axial Transonic Jet, AIAA Paper 2007-3649, May 2007.
5. Papamoschou, D., "Mach Wave Elimination in Supersonic Jets," *AIAA Journal*, Vol. 35, No.10, 1997, pp. 1604-1611.
6. Simmons, R.J., "Design and Control of a Variable Geometry Turbofan with an Independently Modulated Third Stream," Ph.D. Dissertation, The Ohio State University, 2009.
7. Henderson, B., "Aeroacoustics of Three-Stream Jets," AIAA Paper 2012-2159, June 2012.
8. Papamoschou, D. and Debiasi M., "Directional Suppression of Noise from a High-Speed Jet," *AIAA Journal*, Vol. 39, No.3, 2001, pp. 380-387
9. Zaman, K.B.M.Q., "Noise- and Flow-Field of Jets From an Eccentric Coannular Nozzle," AIAA Paper 2004-0005, Jan. 2004.
10. Hill, P.G., and Peterson, C.R., "Mechanics and Thermodynamics of Propulsion," 2nd Ed., Addison-Wesley, 1992.
11. Young, J.B., and Wilcock, R.C., "Modeling the Air-Cooled Gas Turbine: Part 1 – General Thermodynamics," *Journal of Turbomachinery*, Vol. 124, 2002, pp. 207-313.
12. Brear, M.J., Kerrebrock, J.L., and Epstein, A.H., "Propulsion System Requirements for Long Range, Supersonic Aircraft," *Journal of Turbomachinery*, Vol. 128, 2006, pp. 370-377.
13. Papamoschou, D., "Engine Cycle and Exhaust Configurations for Quiet Supersonic Propulsion," *AIAA Journal of Propulsion and Power*, Vol. 20, No. 2, 2004, pp. 255-262.
14. Papamoschou, D., "Acoustic Simulation of Coaxial Hot Air Jets Using Cold Helium-Air Mixture Jets," *Journal of Propulsion and Power*, Vol. 23, No. 2, 2007, pp. 375-381.
15. Sivells, J.C., "A Computer Program for the Aerodynamic Design of Axisymmetric and Planar Nozzles for Supersonic and Hypersonic Wind Tunnels," AEDC-TC-78-63, 1978.
16. Papamoschou, D., "New Method for Jet Noise Suppression in Turbofan Engines," *AIAA Journal*, Vol. 42, No.11, 2004, pp. 2245-2253.